Radiative properties of neutral germanium obtained from excited-state lifetime and branching-ratio measurements and comparison with theoretical calculations

Z.-S. Li, J. Norin, A. Persson, C.-G. Wahlström, and S. Svanberg
Department of Physics, Lund Institute of Technology, P.O. Box 118, S-221 00 Lund, Sweden

P. S. Doidge
Varian Australia Party Limited, P.O. Box 222, Clayton South, Victoria 3169, Australia

E. Biémont
Institut d'Astrophysique, Université de Liège, 5 Avenue de Cointe, B-4000 Liège, Belgium
and Astrophysique et Spectroscopie, Université de Mons–Hainaut, 15 Rue de la Halle, B-7000 Mons, Belgium
(Received 2 November 1998)

Using time-resolved UV laser-induced fluorescence from a laser-produced plasma, natural radiative lifetimes have been measured for 21 levels of Ge I belonging to the odd-parity $4p4d$, $4p5d$, and $4p6s$ configurations. Stimulated Brillouin scattering in water has allowed us to compress Nd:YAG laser pulses pumping a dye laser (where YAG denotes yttrium aluminum garnet), thus yielding 1-ns tunable laser pulses to enable accurate measurements of short lifetimes. Branching ratios of Ge I have been measured by inductively coupled plasma emission spectrometry, the intensity calibration being performed by means of Ar lines emitted by a hollow-cathode lamp. The experimental lifetimes and branching ratios have been combined in order to provide a set of accurate transition probabilities for the $4p$-$5s$ and $4p$-$4d$ transitions. A relativistic Hartree-Fock calculation, taking configuration-interaction and polarization effects into account, has been combined with a least-squares optimization procedure of the Slater and spin-orbit integrals in order to test the ability of this approach to correctly predict radiative properties of the group-IV elements. Good agreement between experimental and theoretical transition probability values has been achieved for most of the transitions considered. [S1050-2947(99)08206-2]

PACS number(s): 32.70.Cs, 42.62.Fi

I. INTRODUCTION

In a previous paper [1] we have investigated some odd-parity levels of atomic lead, an atom characterized by a p^2 electronic configuration in the ground state. Observed lifetime values along Rydberg series have been compared with calculations using the relativistic Hartree-Fock (HFR) method. Fair agreement has been achieved for most of the levels. In the present paper we study the spectrum of a lighter group-IV element, germanium. Ge I is observed in astrophysics in the spectra of Ap and Bp stars (see, e.g., Ref. [2] or [3]) and in the solar photosphere (see, e.g., Ref. [4]) and the determination of the chemical composition of the stars depends in a sensitive way on the availability of accurate transition probabilities. In a previous paper [5] the solar implications of a scale of f values for the $4p^2$-$4p5s$ transitions have been discussed and this has led to an improved value of the photospheric abundance of germanium, which is now in agreement with the meteoritic result. In the present paper we focus on radiative lifetimes of the $4p4d$, $4p5d$, and $4p6s$ levels of Ge I and on transitions originating from the $4p4d$ and $4p6s$ upper configurations.

The energy levels of Ge I, compiled by Sugar and Musgrove [6], are essentially based on the work of Brown, Tilford, and Ginter [7] and Humphreys and Andrew [8]. *LS*-coupling designations have been adopted for the $4p^2$, $4p5s$, $4p4d$, and $4p5d$ configurations, while jj coupling was found to be more adequate for describing the $4p6s$

configuration. While the low-energy levels of Ge I are rather well established, this is certainly not the case for the radiative properties (f values, transition probabilities, and lifetimes). These atomic data, which are rather poorly known, are nevertheless of crucial importance not only for astrophysics but also for laboratory spectroscopy in order to provide more insight into the atomic properties of neutral germanium. The earliest natural radiative lifetime measurements of neutral germanium were published by Lawrence [9] using the phase-shift method. By crossing a germanium atomic beam with a modulated electron beam, he observed the lifetimes of the $4p5s\ ^3P_2^o$ and $4p5s\ ^1P_1^o$ levels. Beam-foil lifetime measurements of the $4p5s\ ^3P_{2,1,0}^o$ and $4p5s\ ^1P_1^o$ levels were reported by Andersen, Petkov, and Sorensen [10]. Komarovskii and Verolainen [11] published lifetime values for the $4p5s$ configuration levels using the method of delayed coincidence combined with a pulsed-electron beam excitation. Tint, Kono, and Goto [12] measured 12 lifetimes of the $4p5s$ and $4p4d$ configurations with essentially the same method, but using GeH_4 instead of pure Ge for the beam. Up to now, the only laser lifetime measurements are due to Biémont *et al.* [5], who reported, by observing laser-induced fluorescence, accurate lifetimes of selectively excited levels of the $4p5s$ configuration. A theoretical calculation of natural radiative lifetimes of neutral germanium was performed by Holmgren and Garpman [13], using relativistic self-consistent-field wave functions.

In the present work we have performed extensive mea-

surements of natural radiative lifetimes of Ge I using time-resolved laser-induced fluorescence. In order to obtain accurate lifetimes of short-lived states, short-duration excitation laser pulses are needed. We have used the stimulated Brillouin scattering (SBS) technique [14] to produce these short laser pulses. The technique is described in Secs. II–IV.

Branching-ratio measurements have been performed using an inductively coupled plasma (ICP) emission spectrometer, the intensity calibration being made by means of Ar lines emitted by a hollow-cathode lamp. From the combination of the lifetime- and branching-ratio values, it has been possible to derive a set of accurate transition probabilities for the $4p$-$5s$ and $4p$-$4d$ transitions of Ge I. The details of the procedure followed are given in Sec. V.

The HFR approach, taking configuration-interaction and polarization effects into account, has also been used in a semiempirical way for atomic structure calculations in Ge I, the Slater and spin-orbit integrals being adequately adjusted in order to better reproduce the experimental levels. In that way, the ability of the HFR approach to correctly predict radiative properties of the group-IV elements has been tested. The details are provided in Sec. VI. The present sets of theoretical and experimental lifetimes and transition probabilities are discussed in Sec. VII, where they are compared with the previous results.

II. SBS COMPRESSOR

The SBS phenomenon was observed by Chiao, Townes, and Stoicheff [15] by sending maser radiation onto solid quartz and sapphire samples. Numerous studies have been performed since then, both theoretically and experimentally, to try to design a pulse compressor using the SBS phase-conjugated reflection in different gaseous and liquid media [16–20]. Recently, through the work of Schiemann and co-workers [21,22], a convenient SBS compressor based on a liquid medium (water, carbon tetrachloride, or methanol) with a high energy transfer efficiency and a high compression factor came into reality.

A design of the SBS compressor, similar to the one described in Ref. [21], is adopted in the present experiment. A 1-ns-duration laser pulse is obtained by compressing the 8-ns second-harmonic output of a Nd:YAG laser (where YAG denotes yttrium aluminum garnet) with the phase-conjugated SBS reflector. The setup of the laser system combined with the SBS pulse compressor is shown in Fig. 1. The pulse compressor consists of a SBS phase-conjugated reflector, a polarization beam isolator, and a beam expander. The SBS reflector is composed of a 150-cm glass tube serving as an amplifier (A) and a 30-cm glass tube serving as a generator (B). The units are connected to each other by a 15-cm focusing lens. Both tubes are filled with pure water and sealed with anti-reflection coated windows.

Vertically polarized single-mode near Fourier-transform-limited laser radiation emitted from a seeder-injected frequency-doubled Nd:YAG laser (Continuum NY 82-10), with a 400-mJ pulse energy and an 8-ns pulse duration) is sent in the beam expander and made circularly polarized with a quarter-wave plate ($\lambda/4$). This beam is sent through tube A and focused into tube B with a lens (L). The leading edge of the laser pulse injected into tube B starts to be re-
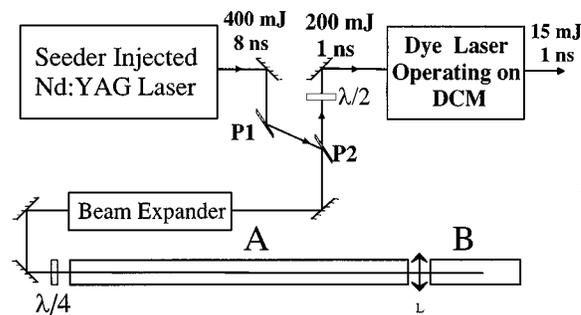
FIG. 1. Laser and SBS compressor arrangement. $\lambda/2$ and $\lambda/4$ are a half-wave and a quarter-wave retarding plate; $P1$ and $P2$ are plate polarizers placed at the Brewster angle; L is a lens of 15 cm focal length.

flected by the acoustic wave in the water when the power is over the threshold. A phase-conjugated reflection wave is then formed before the focus point, which is amplified all the way back by the input beam through tube B to tube A. The reflected phase-conjugated beam absorbs almost all the energy of the input pulse. Due to Rayleigh and Raman scattering in the water and reflective losses in all the optical surfaces, only 50% reflection efficiency and a compression of the pulse to 1 ns can be achieved. The phase-conjugated reflected laser pulse changes to horizontally polarized after passing through a quarter-wave plate ($\lambda/4$) and propagates along exactly the same path as the input beam to the plate polarizer ($P2$). The horizontally polarized beam passes through the plate polarizer ($P2$) [the small reflection by $P2$ is further separated by the plate polarizer ($P1$) to protect the Nd:YAG laser] and changes the polarization direction to the vertical through the half-wave plate ($\lambda/2$) before being sent to pump the dye laser.

The separated 1-ns, 200-mJ pulse at 532 nm was used to pump a dye laser (Continuum ND 60). The SBS compressor was designed to compress the second harmonic of the Nd:YAG laser pulse and the compressed 532-nm radiation pulse could be used to pump several red dyes, enabling a large, flexible, tunable wavelength region. DCM was used for the present experiment, which provides 15-mJ pulse energy at 1-ns duration.

III. EXPERIMENTAL SETUP

The full experimental setup for lifetime measurements is shown in Fig. 2. The radiation from the dye laser was first frequency doubled in a potassium dihydrogen phosphate (KDP) crystal and then mixed with the fundamental frequency in a β-barium borate (BBO) crystal to produce the third harmonic of the dye laser frequency. To enhance the type-I mixing in the BBO crystal, a mechanically compressed quartz plate was placed between the KDP and BBO crystals, which was used to rotate the fundamental and the doubled dye laser radiation to obtain parallel polarization. A detailed description of this procedure can be found in Ref. [23]. In order to obtain the required short laser wavelength down to 193 nm, the first anti-Stokes Raman component in molecular hydrogen was used. By focusing the third harmonic of the dye laser into the hydrogen in the Raman shifter, different orders of Stokes and anti-Stokes scattering
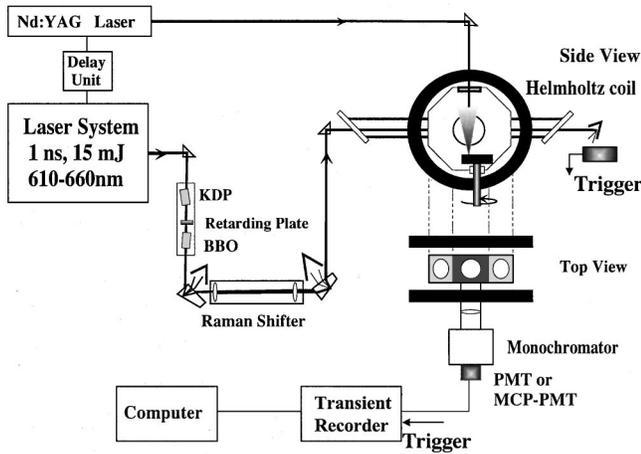
FIG. 2. Experimental setup used in the present experiment.

were produced and favorable components for different excitations were separated by a CaF$_2$ Pellin-Broca prism and sent to cross the atomic beam in the vacuum chamber. The same technique was used earlier for producing 8-ns laser pulses in studies of neutral silver [24] and bismuth [25].

Free germanium atoms were obtained in a laser induced plasma. A 532-nm, 10-ns, (10–20)-mJ laser pulse, provided by a separate 10-Hz Nd:YAG laser (Continuum Surelite), was focused on a rotating metallic germanium target and a plasma with sufficient populations in the ground as well as metastable states of neutral germanium was obtained. The excitation beam passed through the center of the vacuum chamber, about 2 cm above the rotating target. Both Nd:YAG lasers were externally triggered by the same delay unit (Stanford Research Systems Model 535 digital delay generator), which enabled the delay time between the atomization and excitation laser pulses to be varied freely.

Fluorescence photons were collected perpendicular to the two laser beams by a fused silica lens and were appropriately filtered by a $\frac{1}{8}$-m monochromator, which had a resolution of 6.4 nm/mm. A Hamamatsu 1564U microchannel-plate (MCP) photon multiplier [200-ps rise time; (200–600)-nm spectral response region] or a Hamamatsu R1220 photomultiplier tube (PMT) [2.2-ns rise time; (120–300)-nm spectral

response region] was used alternatively depending on the fluorescence wavelength. The data acquisition was performed by a digital transient recorder (Tektronix Model DSA 602) that had a 1 GHz bandwidth and worked in a real-time mode with a 2 gigasample/s sampling rate. The averaged time-resolved fluorescence decay curves were transferred to a personal computer and lifetime evaluations were performed immediately.

IV. MEASUREMENTS AND RESULTS

The energy states of neutral germanium relevant to the present experiments are shown in Fig. 3. In the laser-induced plasma, all the metastable states of the $4p^2$ configuration were sufficiently populated, which allowed the selection of appropriate transitions for exciting the desired upper levels. The transitions used in the present experiment are indicated in Table I. The different schemes of laser excitation, the corresponding wavelengths, and the wavelengths of the observed fluorescence are indicated in Table I for each level.

Time-resolved laser spectroscopy was used to obtain reliable lifetime values under appropriate experimental conditions. A Helmholtz coil system provided a sufficiently high magnetic field to wash out quantum beats due to Zeeman splitting for long-lived states. Flight-out-of-view effects were investigated by changing the position and slit width of the monochromator; no resolvable effects were observed. To make sure that the measured lifetimes are not affected by radiation trapping or by collisional quenching in the laser-induced plasma, different delay times between the atomization laser pulse and the excitation laser pulse were used in the measurements. We found that with a sufficiently long delay time after the ablation pulse (about 10 μs), the evaluated lifetimes were almost constant. The same phenomenon has also been observed in the Pb I [1] and S I work [26,27]. In the practical measurements, the plasma density and excitation laser power were effectively lowered to make sure that the number of photons recorded in each transient was small enough to exclude influence from a nonlinear response of the detector. Four thousands shots were accumulated for each recording to make a smooth curve. For the levels that have a lifetime longer than 5 ns, a least-squares exponential fitting
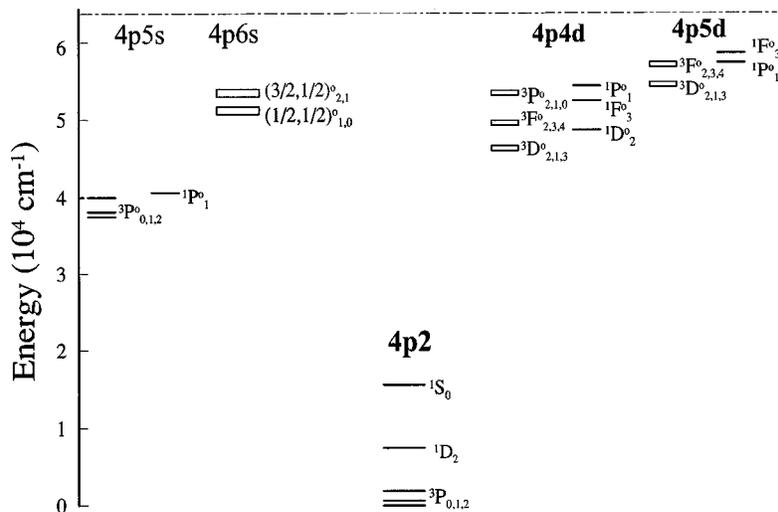
FIG. 3. Partial energy-level diagram for neutral germanium.

TABLE I. Odd-parity levels of Ge I: levels for which the lifetimes have been measured, excitation scheme, and observed fluorescence. The excitation beam was the third harmonic of a dye laser operated with DCM dye, while for shorter wavelengths marked by AS, the first anti-Stokes shift in H_2 has been used. R indicates that the detector used was a Model R1220 (2.2 ns rise time), while for the other states an R1564U detector (0.2 ns rise time) was used.

State	Energy (cm^{-1})	Excitation		Fluorescence	
		Lower state	λ (nm)	Lower state	λ (nm)
$4d\ ^1D_2^o$	48 480.05	$4p^2\ ^3P_2^o$	212.45	$4p^2\ ^1D_2^o$	242
$4d\ ^3D_2^o$	48 882.26	$4p^2\ ^3P_2^o$	210.64	$4p^2\ ^3P_1^o$	207
$4d\ ^3D_1^o$	48 962.78	$4p^2\ ^3P_2^o$	210.29	$4p^2\ ^3P_0^o$	204
$4d\ ^3D_3^o$	49 144.40	$4p^2\ ^3P_2^o$	209.49	$4p^2\ ^1D_2^o$	238
$4d\ ^3F_2^o$	50 068.95	$4p^2\ ^3P_2^o$	205.51	$4p^2\ ^3P_1^o$	202
$4d\ ^3F_3^o$	50 323.47	$4p^2\ ^3P_2^o$	204.44	$4p^2\ ^1D_2^o$	231
$4d\ ^3P_2^o$	51 437.80	$4p^2\ ^3P_1^o$	196.53 AS	$4p^2\ ^1D_2^o$	226
$4d\ ^3P_1^o$	51 705.02	$4p^2\ ^3P_1^o$	195.51 AS	$4p^2\ ^1S_0^o$	283
$4d\ ^3P_0^o$	51 978.15	$4p^2\ ^3P_1^o$	194.54 AS	$4p^2\ ^3P_1^o$	194 R
$6s(\frac{1}{2},\frac{1}{2})_1^o$	52 148.73	$4p^2\ ^3P_2^o$	197.08 AS	$4p^2\ ^1S_0^o$	279
$6s(\frac{1}{2},\frac{1}{2})_0^o$	52 170.50	$4p^2\ ^3P_1^o$	193.75 AS	$4p^2\ ^3P_1^o$	194 R
$4d\ ^1F_3^o$	52 592.22	$4p^2\ ^1D_2^o$	219.94	$4p^2\ ^1D_2^o$	220
$4d\ ^1P_1^o$	52 847.22	$4p^2\ ^1D_2^o$	218.71	$4p^2\ ^1S_0^o$	274
$6s(\frac{3}{2},\frac{1}{2})_2^o$	53 911.62	$4p^2\ ^1D_2^o$	213.74	$4p^2\ ^3P_2^o$	190 R
$6s(\frac{3}{2},\frac{1}{2})_1^o$	54 174.93	$4p^2\ ^1D_2^o$	212.54	$4p^2\ ^1S_0^o$	265
$5d\ ^3D_2^o$	55 372.61	$4p^2\ ^1D_2^o$	207.27	$4p^2\ ^3P_1^o$	182 R
$5d\ ^3D_1^o$	55 474.67	$4p^2\ ^1D_2^o$	206.82	$4p^2\ ^1S_0^o$	256
$5d\ ^3D_3^o$	55 718.60	$4p^2\ ^1D_2^o$	205.79	$4p^2\ ^1D_2^o$	206
$5d\ ^3F_2^o$	55 686.70	$4p^2\ ^1D_2^o$	205.92	$4p^2\ ^3P_2^o$	184 R
$5d\ ^1P_1^o$	58 058.06	$4p^2\ ^1D_2^o$	196.34 AS	$4p^2\ ^1D_2^o$	196 R
$5d\ ^1F_3^o$	58 093.35	$4p^2\ ^1D_2^o$	196.20 AS	$4p^2\ ^1D_2^o$	196 R

procedure of the recorded fluorescence has been used to evaluate the lifetimes. Only that part of the curves that was recorded after the turn off of the laser pulse was used in the fit. The starting point of the fit was varied to make sure that no deviations from an exponential shape of the signal influenced the measurements. The lifetimes shorter than 5 ns were evaluated by fitting a convolution of an exponential and the laser pulse, which was accumulated with the same detection system by inserting a metal rod at the interaction spot of the excitation laser and the plasma (the ablation laser was turned off while accumulating the laser pulses). The role of the metal rod is to scatter the laser light into the monochromator. Special attention was paid to the saturation conditions of the excitation of the short-lived states. Different excitation laser power (obtained by inserting neutral density filters in the laser beam) were used to make sure that saturation did not influence the measured lifetime values evaluated by the convolution fitting. An example for the $4d\ ^1F_3^o$ level is shown in Fig. 4. For each state, about 30 curves were recorded for different experimental conditions. The lifetimes values, evaluated from the curves recorded under proper experimental conditions, were averaged to obtain final results. These data are listed in Table II, where they are compared with previous experimental results but also with the semi-empirical results obtained in the present work (see Sec. VI). One standard deviation in the data and an allowance for small residual systematic errors are included in the quoted error bars.

V. BRANCHING-RATIO MEASUREMENTS

A. Experiment

An ICP emission spectrometer (Varian Australia Pty. Ltd., Mulgrave, Victoria, Australia), with ''radial'' (side-on) viewing of the plasma discharge sustained in argon, was used for the branching-ratio (BR) measurements. The instrument was equipped with a scanning monochromator, 0.75 m focal length, with an 1800-lines/mm holographic grating (illuminated area $90 \times 80\ mm^2$) in a symmetrical Czerny-Turner mount. The grating could be used in multiple orders, provided the condition $950\ nm \geqslant n\lambda$, with n the order num-
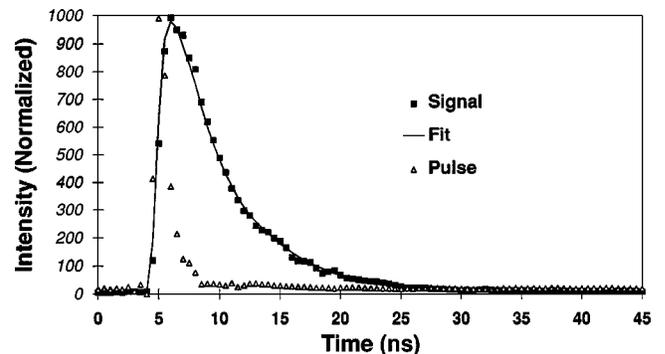
FIG. 4. Recording of a time-resolved fluorescence signal of the $4d\ ^1F_3^o$ level, the laser pulse, and a convolution fit of the laser pulse with a $\tau = 3.8$ ns exponential.

TABLE II. Ge I: observed and calculated radiative lifetimes and comparison with previous results.

State	Energy (cm^{-1})	τ (ns) This work Expt.	HFR	Others (Expt.)
$5s\ ^3P_0^o$	37 451.69	4.81(0.14)[a]	4.30	4.9(0.6),[b] 3.6(0.4),[c] 6.0(0.9),[d] 6.0(0.5)[e]
$5s\ ^3P_1^o$	37 702.31	4.68(0.20)[a]	4.13	4.4(0.6),[b] 3.7(0.5),[c] 6.8(0.7)[e]
$5s\ ^3P_2^o$	39 117.90	4.50(0.18)[a]	3.94	4.2(0.5),[b] 4.0(0.4),[c] 7.4(0.6)[e]
$5s\ ^1P_1^o$	40 020.56	4.23(0.14)[a]	3.81	4.0(0.3),[b] 3.9(0.5),[c] 4.4(0.7),[d] 6.2(0.6)[e]
$4d\ ^1D_2^o$	48 480.05	13.2(0.8)	11.91	13.8(0.7)[b]
$4d\ ^3D_2^o$	48 882.26	6.1(0.4)	5.07	6.9(0.3)[b]
$4d\ ^3D_1^o$	48 962.78	4.3(0.4)	3.72	5.0(0.8)[b]
$4d\ ^3D_3^o$	49 144.40	6.0(0.4)	4.74	5.3(0.5)[b]
$4d\ ^3F_2^o$	50 068.95	13.1(0.5)	18.64	15.2(0.8)[b]
$4d\ ^3F_3^o$	50 323.47	10.8(0.5)	16.71	
$4d\ ^3P_2^o$	51 437.80	7.5(0.5)	6.34	7.5(0.7)[b]
$4d\ ^3P_1^o$	51 705.02	8.6(0.4)	6.06	
$4d\ ^3P_0^o$	51 978.15	8(1)	5.15	
$6s(\frac{1}{2},\frac{1}{2})_1^o$	52 148.73	10.5(0.5)	10.65	
$6s(\frac{1}{2},\frac{1}{2})_0^o$	52 170.50	13(2)	29.18	
$4d\ ^1F_3^o$	52 592.22	3.8(0.3)	2.62	3.9(0.3)[b]
$4d\ ^1P_1^o$	52 847.22	9.8(0.5)	6.38	10.3(0.8)[b]
$6s(\frac{3}{2},\frac{1}{2})_2^o$	53 911.62	13(2)	16.27	
$6s(\frac{3}{2},\frac{1}{2})_1^o$	54 174.93	11.1(0.9)	9.16	
$5d\ ^3D_2^o$	55 372.61	45(3)	70.16	
$5d\ ^3D_1^o$	55 474.67	29.3(1.2)	13.37	
$5d\ ^3D_3^o$	55 718.60	25.5(1.2)	14.53	
$5d\ ^3F_2^o$	55 686.70	56(3)	61.70	
$5d\ ^1P_1^o$	58 058.06	24(2)	8.45	
$5d\ ^1F_3^o$	58 093.35	13(2)	6.93	

[a]Biémont *et al.* [5] (time-resolved laser-induced fluorescence).
[b]Tint, Kono, and Goto [12] (delayed coincidence technique).
[c]Andersen, Petkov, and Sorensen [10] (beam-foil spectroscopy).
[d]Lawrence [9] (phase-shift method).
[e]Komarovskii and Verolainen [11] (delayed coincidence technique).

ber, was satisfied; use of multiple orders was advantageous in the far-UV region in cases where blends of lines occurred and all lines studied were measured in all possible orders of the grating as a check on the occurrence of blends. The exit slit width of 19 μm provided a spectral bandpass, in first order, approximately equal to 0.018 nm, while in fourth order, the highest practical order, the spectral bandpass was approximately 0.005 nm. As the spectrum of Ge I is quite sparse, this resolution was adequate for measurements made in first and second orders, which were preferred for reasons of signal-to-noise ratio. Aqueous samples were introduced to the plasma with the standard nebulizer and spray chamber.

Two photomultipliers were used: a Hamamatsu solar-blind R166-04 below 300 nm and a Hamamatsu multialkali (R446) above 300 nm. Order-sorting filters are also used above 231 nm to minimize order overlaps. Correction for the spectral continuum (''background''), on which the emission lines are superimposed, was applied automatically by the instrument's controlling software. Typically, only several min-

utes were required for the measurement of all lines from a given excited level; integration times of 5–10 s were used for nearly all lines, three replicate measurements were made on each line, and the grating was capable of slewing from one wavelength to the next in a run in several seconds.

Hollow-cathode lamps were mounted in the plasma torch compartment, in place of the torch, and were powered from either a dc or an ac power supply. An Ar-filled hollow-cathode lamp with Al cathode, operated at currents of 4–12 mA, was used for the intensity calibration. No significant effects ($>$10%) of lamp current, in terms of variations in the ratios of lines with common upper levels, were observed with any of the levels of Ar (I and II) that were studied, though the effect of lamp current was not studied for all the levels measured. A Varian Cary 4 UV-visible spectrophotometer with nitrogen-purged sample compartment was used to measure the transmittance of a hollow-cathode lamp window. Some measurements of Ge I intensities were also made with a hollow-cathode lamp as the source; a Ne-filled Ge

hollow-cathode lamp (Varian Australia Pty. Ltd.) was operated at currents of 3–12 mA.

Measurements of Ar II lines were limited to the air region (greater than approximately 186 nm); although the spectrometer had a vacuum path that allowed measurement to 160 nm, the intensity calibration had to be effected with a hollow-cathode lamp mounted in the plasma torch compartment and the purging of this compartment with Ar was not effective enough to allow the use of lamps below the wavelength at which absorption by air became limiting.

B. Intensity calibration

Over most of the spectral region covered by the measurements described here (190–800 nm), the intensity calibration was carried out with the Ar I and Ar II branching ratios reported in several papers [28–30]. Most of the 98 Ar II levels, totaling 399 lines, reported by Hashiguchi and Hasikuni [28] were measured at least once, although for several of the levels, especially those with branches in the region 220–240 nm, many branches were too weak to be useful; many of the 56 levels of Ar I and II listed by Whaling, Carle, and Pitt [29] were also measured. All but one of nine near-vacuum-ultraviolet Ar II levels measured by Siems *et al.* [30] were measured, in all cases more than once, and, for most levels, three times.

The basic approach was the same as that used in Ref. [28]: When the physical line width is somewhat less than the spectrometer bandpass, the latter dominates the line profile and the peak line intensity is proportional to the integrated line intensity $\int I(\lambda)d\lambda$, the latter actually being proportional to the branching ratio. This approach was adopted in the present study. It is justified from a comparison of the spectral bandpass used in the present work with the presumed Ar linewidths: Ar II lines from the high-current hollow-cathode discharge used in Ref. [28] were reported to be 3 pm wide (full width at half maximum) and lines emitted by the lamp used in the present work were probably narrower still, because of its lower operating current, compared to that used in Ref. [28].

Calibration in the region 295–375 nm was also carried out with branching ratios derived from the absorption *f* values of Ni I reported by Blackwell *et al.* [31]. As in the case of Fe I [32], these values can probably be considered sufficiently accurate to be used as branching ratios.

The validity of the approach described here for BR determination is supported by comparisons of measured BRs of Fe I with values derived from reports of Blackwell, Petford, and Simmons [32], and O'Brian *et al.* [33]; a more detailed discussion of this aspect of the work will be given elsewhere [34].

As mentioned, Ar II lines in the region 220–240 nm were often very weak in the hollow-cathode spectrum. This necessitated estimation of the response around 230 nm from changes in the intensity of the plasma ''background,'' the latter fitted to a Planck blackbody function at a temperature derived from branching-ratio measurements [34].

C. General considerations

Whereas lines of the $4p5s$ levels could be measured with a hollow-cathode lamp, lines from $4p4d$ levels were nearly all too weak in the hollow-cathode spectrum to be measured. Branching ratios of the lines from $4p4d$ levels were therefore all measured with the Ar ICP.

Attempts to detect the 800.111-nm line from the level $4p4d\ ^3D_1^o$ (48 962.78 cm^{-1}) were unsuccessful, even at the highest concentration of Ge introduced into the ICP, and this line has been ignored in the calculations of branching fractions from this level. The problem with detecting this line was almost certainly due to a combination of low PMT (and grating) response in this wavelength region and an inherently weak line. This line was assigned a very low intensity by Andrew and Meissner [35], though other lines of Ge I above 800 nm were assigned very much higher intensities by them; this fact would seem to justify a neglect of this line in the calculation of the branching fractions.

For one other line from this level, 306.7021 nm, the intensity measurement with the ICP was difficult because the line was both very weak and partially blended with a line (306.7240 nm) of the $A\ ^2\Sigma \rightarrow X\ ^2\Pi$ system of OH present in the background spectrum of the ICP, OH lines being fairly strong because of the introduction of sample as aqueous aerosol. It was necessary to measure this line in either the second or the less efficient third grating order and convert the intensities to effective ones for first or second order; this introduced an extra (small) error. With the very weak 238.947-nm line from the same level, intensities were low because of the spectrometer's poorer efficiency in this region. The BRs of this and the 306.70-nm line have then been given ±25% errors.

The Ar ICP is optically thin, thus minimizing the effects of self-absorption on measured ICP intensities [33]. Nevertheless, checks of the constancy of the ratios of intensities of lines (with common upper levels), needed to obtain accurate branching ratios, were made. This was done simply by varying the concentration of seed element (Ge) aspirated into the plasma over approximately two orders of magnitude.

With the scanning spectrometer used here, checks were needed to ensure that source drift during measurements was not a problem. The ICP is an exceptionally stable source and intensities can be stable to ±1% or less over a period of 1 h or more, so that drift of the ICP was not a problem. In any case, all levels of Ge I were measured at least twice and mean relative intensities were used. With the hollow-cathode lamp, drift can be a more serious problem and it was checked by monitoring a strong Ar II line (427.75 nm) at regular intervals and remeasuring the Ar II lines if this had drifted by more than a few percent.

To minimize any effects of long-term drift of the spectrometer response on the measured BRs of Ge I, response curves were measured in the far-UV region (where instrument-response drift tends to be most serious) before and after the measurements of Ge I intensities were made. Typically, there was no more than a 6–7% difference in relative response at 220 nm, relative to the peak in the response curve at approximately 200 nm, between the two sets of measurements (or about ±3% about the mean). Further details of precautions adopted to minimize effects of drift in spectrometer response and the transmission of hollow-cathode lamp windows will be given elsewhere [34].

D. Estimation of errors

The intensities of most of the Ge I lines, as measured with the ICP, were sufficiently high that the photon shot noise of the measurement was very small and its effect on the final uncertainties in the branching ratio could be neglected. The largest contribution to the errors in the measured Ge I branching ratios derives from the uncertainty in the intensity calibration. This uncertainty is in fact difficult to estimate. O'Brian *et al.* [33] noted that the response function of their Fourier-transform spectrometer contributed to uncertainties in the branching ratio in a complex way and assumed that the magnitude of the branching-ratio error could be calculated as directly proportional to the wavelength separation of the lines, with a constant of 0.001% per wave number separation; for lines at 200 and 400 nm, with no response difference between them, an error in the branching ratio of 25% would follow.

In the present work a different approach was adopted, based partly on comparison of measured BRs of Fe I with published data and partly on the spectrometer characteristics. A comparison of results for Fe I lines in the region 295–460 nm, measured by the present approach, for lines with branching ratios given in Ref. [33], or with relative f values reported by Blackwell, Petford, and Simmons [32], indicated that the errors, as measured by the difference between results with the present approach and literature values, were well within ±5%.

The BR uncertainties were also affected by the necessity to cover a wide wavelength range by connecting a graph of response measured in one region (with a particular grating order and PMT) to that measured for another region (perhaps with different order and PMT). This reflected, in part, a characteristic of the spectrometer: In terms of signal-to-noise ratio, first order was preferred up to approximately 220 nm, second order from approximately 220 nm up, while first and second orders were equally good from approximately 300 nm to nearly 400 nm. The overlap of calibration graphs gave rise to the possibility of an error in the scaling of one graph to another. This was estimated as amounting to as much as ±5%.

In general, the levels analyzed had few branches, with branching characterized by two or three lines fairly close to one another, usually involving the ground-level terms $4p\ ^3P^o_{0,1,2}$ and with at least one other line having a lower level corresponding either to $4p\ ^1D^o_2$ at 7125 cm^{-1} or to $4p\ ^1S^o_0$ at 16 367 cm^{-1}. Because of the nature of the branching, it was therefore considered that an adequate estimation of the maximum errors would be arrived at by assuming an error of ±2–5% for stronger lines close to one another and ±10% for stronger lines far apart in the spectrum or for a weak line relative to a stronger line. These are considered to be maximum likely errors, based on experience in measuring lines with known BRs, as described elsewhere [34] for Fe I and other selected atoms.

The BRs with their uncertainties are given in column 5 of Table III. Combined with the laser lifetimes measured in the present work or in Ref. [5], they provide the f values and transition probabilities, with their uncertainties, as reported in the last columns of the same table.

VI. HFR CALCULATIONS

Semiempirical transition probabilities have been calculated in the present work using the well-known computer code written by Cowan [36] within the framework of the HFR approach. As we were interested in transitions involving low excitation levels, the configuration sets have been limited to the Layzer complexes with $n \leq 6$. In fact, the configuration interaction has been considered using the following final set of 33 configurations: $4s^2 4p^2 + 4s^2 4pnp$ ($n = 5,6$) $+ 4s^2 4pnf$ ($n = 4-6$) $+ 4s^2 4d^2 + 4s^2 5s^2 + 4s^2 5p^2 + 4s^2 5d^2 + 4s4p^2 5s + 4s4p^2 nd$ ($n = 4,5$) $+ 4s^2 4d5s + 4s^2 4d5d + 4s^2 5s5d + 4s^2 5p5f$ (even parity) and $4s^2 4pns$ ($n = 5,6$) $+ 4s^2 4pnd$ ($n = 4-6$) $+ 4s4p^3 + 4s4p^2 5p + 4s4p^2 nf$ ($n = 4,5$) $+ 4s^2 4dnf$ ($n = 4,5$) $+ 4s^2 5s5p + 4s^2 5s5f + 4s^2 5p5d + 4s^2 5d6p + 4s^2 5d5f$ (odd parity). In order to reduce as much as possible the discrepancies between computed and experimental energy levels, the HFR technique was used in combination with a least-squares optimization process of the Slater integrals. The original set of configurations retained in Ref. [5] was somewhat reduced for computational reasons, but this reduction was compensated for by the introduction of the fitting procedure not considered previously. The experimental levels have been taken from the compilation of Sugar and Musgrove [6], the two levels of the $4p6d$ configuration at 61 091.5 and 61 268.4 cm^{-1} being excluded from the fit. All the F^k, G^k, and R^k integrals not adjusted in the fitting procedure were scaled down by a factor of 0.85, while the spin-orbit integrals ζ_{nl}, characterized by small numerical values, were used without scaling. Due to space limitations, the details of the calculations will not be given here, but the numerical values adopted for the Slater parameters, for the spin orbit, and for the configuration interaction integrals as well as the composition of the levels can be obtained upon request from the authors.

The present calculations are susceptible to core-polarization effects, particularly for transitions involving low excitation energies. According to a procedure described by Migdalek and Baylis [37], the core-valence correlation has been approximated by a core-polarization potential depending upon two parameters, i.e., α_d, the static dipole polarizability of the core, and r_c, the cutoff radius that is arbitrarily chosen as a measure of the size of the ionic core. This parameter is usually taken as the expectation value of r for the outermost core orbital. Cowan's code has been corrected to take polarization into account and the procedure has appeared successful for providing accurate f values in heavy ions such as Yb II and Tm II (see Refs. [38, 39]). For Ge I, the dipole polarizability of the ionic core α_d has been chosen to be equal to $4.05a_0^3$ for the $3d^{10}4s$ configuration, which corresponds to the value reported by Fraga, Karwowski, and Saxena [40]. For the cutoff radius r_c we used the average value $\langle r \rangle$ for the outermost core orbital as calculated by the Cowan code, i.e., $\langle r \rangle = 1.897a_0$.

The HFR lifetime values are given in column 4 of Table II. It is seen that using the fitting procedure the present HFR lifetime values for the $4p5s$ levels are somewhat larger than the theoretical results obtained in Ref. [5], where more cor-

relation effects were included but where the calculations were performed in an *ab initio* way. As a consequence, the agreement between theory and experiment is somewhat improved for the $4p5s$ levels. In fact, the agreement between the HFR results and the laser lifetimes is good for most of the levels, larger discrepancies appearing only for the $4p6s(\frac{1}{2}, \frac{1}{2})_0^o$ level and also for some levels of the configuration $4p5d$. As cancellation effects do not play a role here, these discrepancies are probably related to neglected configuration-interaction effects with higher members of the Rydberg series and also to the fact that the fitting procedure is less satisfying for the odd levels than for the even ones, indicating that some level assignments or level values could be in need of revision.

The HFR oscillator strengths ($\log_{10}gf$) and transition probabilities (A_{ki} in $10^8 \, \text{s}^{-1}$), calculated with the optimized parameters, are reported in columns 3 and 4 of Table III for the UV $4p^2$-$4p5s$ and $4p^2$-$4p4d$ transitions. Only one transition is affected by cancellation effects (severe destructive interferences in the calculation of the line strengths, the cancellation factor, as defined by Cowan [36], being smaller than 0.0050) and it is indicated by footnote e in the table. The transition probabilities obtained with the fitted parameters have been slightly modified by using a normalization factor for each level deduced by imposing an agreement between the calculated lifetime values and the observed ones. This has introduced a change in the oscillator strengths of the order of 0.05 dex (i.e., in a logarithmic scale) for most of the levels, the change being somewhat larger for a few levels (see Table II). It is seen that the agreement between the normalized theoretical transition probabilities and the experiment is excellent for the $4p$-$5s$ and for most of the $4p$-$4d$ transitions. Some large discrepancies are observed, however, for a number of $4p$-$4d$ weak intercombination transitions. This reflects the sensitivity of these transitions to small changes in the eigenvector compositions that are directly related to the choice of the configurations introduced in the model. The general agreement is nevertheless gratifying because, for a heavy neutral element such as Ge I, both relativistic effects and correlation contributions must be simultaneously considered and render accurate calculations extremely difficult.

VII. COMPARISON WITH PREVIOUS RESULTS

A. Radiative lifetimes

The laser lifetimes obtained in the present work and the HFR results, calculated as described in Sec. VI, are compared in Table II with previously published experimental results. For the $5s$ $^{1,3}P^o$ levels, the laser measurements are in nice agreement with the delayed-coincidence results of Tint, Kono, and Goto [12] while, for the same levels, the HFR results appear systematically and coherently smaller than the experiment, the mean ratio being 1.126 ± 0.014. Similar findings have been reported previously in different ions when comparing HFR lifetimes with accurate beam-laser measurements (see, e.g., the cases of Fe II [46], Cr II [47], and Ag II [48]). The beam-foil results of Andersen, Petkov, and Sorensen [10] are systematically lower than the laser measurements, but should be less accurate. The delayed-coincidence

results of Komarovskii and Verolainen [11], on the other hand, are considerably higher than all the other experimental results, which seems to indicate systematic errors in their measurements.

For the levels of the $4p4d$ configuration, the only possible comparison is with the measurements of Tint, Kono, and Goto [12]. As seen from Table II, the present measurements are in good agreement with the delayed-coincidence results. The HFR results agree also rather well with the measurements of Tint, Kono, and Goto, the largest discrepancy appearing for the $4d$ $^1P_1^o$ level.

B. Oscillator strengths

The HFR oscillator strengths, calculated in the present work with the optimized parameters and normalized according to the procedure described in Sec. VI, are reported in Table III, where they are compared with the experimental results deduced from our laser and branching-ratio measurements. The latter results are also compared in Table III with previous measurements. The comparison is limited to the $4p$-$4d$ transitions, the $4p$-$5s$ transition array having been discussed previously (see Ref. [5]).

Emission measurements have been reported by Lotrian *et al.* [41] for 27 transitions of Ge I. Branching ratios have been measured by these authors in the spectral range 190–470 nm and the absolute scale for the transition probabilities has been established on the basis of the beam-foil lifetime measurements of Andersen, Petkov, and Sorensen [10]. The agreement with our experimental f values is satisfying in the case of the $4p^2$-$4p5s$ transitions (the mean deviation is only 0.03 dex for 13 transitions), but large discrepancies are observed for some lines (e.g., for $\lambda = 208.602$ and 282.901 nm).

Relative transition probabilities of the $4p^2$-$4p5s$ and $4p^2$-$4p4d$ transition arrays have been measured in emission by Pokrzywska *et al.* [44] with a wall-stabilized arc. The results have been put on an absolute scale using the beam-foil lifetimes measured by Andersen, Petkov, and Sorensen [10]. More recently, the results of Ref. [44] have been revised by Musiol *et al.* [45], who used a similar technique (wall-stabilized arc) and normalized their results with the delayed-coincidence measurements of Tint, Kono, and Goto [12]. The results of Musiol *et al.* agree very well with our measurements for the eleven $4p$-$4d$ transitions (the mean deviation $\bar{\Delta}$ is lower than 0.01 dex) if we exclude from the mean the wavelength at 210.227 nm where the discrepancy is larger by one order of magnitude.

Some transitions of Ge I have been considered by Slavenas [43] using Rozhdestvenskii's hook method. Normalizing Slavenas's results on the basis of the $4p$ $^1D_2$-$5s$ $^1P_1^o$ transition at 303.9067 nm ($\log_{10}gf = -0.07$) leads to $\log_{10}gf = -0.60$ for the $4p$ $^1D_2$-$4d$ $^1D_2^o$ transition, which differs by 0.20 dex from our measurement.

We give also in Table III the arc measurements of Corliss and Bozman [42]. These results are given for completeness only because it is now well established that these emission measurements are affected by erratic errors, which sometimes are rather large.

VIII. CONCLUSIONS

Radiative lifetimes have been measured for 21 levels belonging to the odd-parity $4p4d$, $4p5d$, and $4p6s$ levels of

TABLE III. Ge I: observed wavelengths (in nm), HFR oscillator strengths ($\log_{10}gf$), and transition probabilities (A in 10^8 s^{-1}) (this work), experimental branching ratios (BR), transition probabilities (A in 10^8 s^{-1}), oscillator strengths ($\log_{10}gf$) (this work) and comparison with previous results. The HFR calculations have been normalized with the measured laser lifetimes obtained in the present work (see the text).

	HFR			Experiment		
Transition	λ (expt.)[a] (nm)	$\log_{10}gf$	A (10^8 s^{-1})	BR	$\log_{10}gf$	A (10^8 s^{-1})
			$4p^2$-$4p5s$			
$^3P_0$-$^1P_1^o$	249.7963	-1.43	0.131	0.0464(46)	-1.51	0.110(11)
$^3P_1$-$^1P_1^o$	253.3231	-1.48	0.113	0.0362(36)	-1.61	0.0856(89)
$^3P_2$-$^1P_1^o$	258.9188	-1.80	0.052	0.0168(17)	-1.92	0.0397(41)
$^3P_1$-$^3P_2^o$	259.2534	-0.53	0.592	0.272(14)	-0.52	0.604(39)
$^3P_2$-$^3P_2^o$	265.1172	-0.07	1.620	0.721(14)	-0.07	1.60(7)
$^3P_0$-$^3P_1^o$	265.1568	-0.70	0.623	0.325(16)	-0.66	0.694(46)
$^3P_1$-$^3P_1^o$	269.1341	-0.85	0.424	0.221(11)	-0.81	0.473(31)
$^3P_1$-$^3P_0^o$	270.9624	-0.64	2.078	1.000	-0.64	2.08(6)
$^3P_2$-$^3P_1^o$	275.4588	-0.56	0.800	0.371(19)	-0.57	0.792(52)
$^1D_2$-$^1P_1^o$	303.9067	-0.09	1.948	0.861(14)	-0.07	2.04(5)
$^1D_2$-$^3P_2^o$	312.4816	-2.02	0.013	0.007 15(72)	-1.93	0.0159(17)
$^1D_2$-$^3P_1^o$	326.9489	-0.87	0.275	0.0806(81)	-1.08	0.172(19)
$^1S_0$-$^1P_1^o$	422.6563	-1.01	0.120	0.0399(40)	-1.12	0.0943(98)
$^1S_0$-$^3P_1^o$	468.5829	-1.83	0.015	0.002 33(23)	-2.31	0.004 98(54)

	HFR		Experiment			
Transition	λ (expt.)[a] (nm)	$\log_{10}gf$	A (10^8 s^{-1})	BR	A (10^8 s^{-1})	$\log_{10}gf$	Previous ($\log_{10}gf$)
				$4p^2$-$4p4d$			
$^3P_0$-$^1P_1^o$	189.2247[b]	-1.54	0.176	<0.001			
$^3P_1$-$^1P_1^o$	191.2406	-1.68	0.125	0.0334(33)	0.0341(37)	-2.25	
$^3P_0$-$^3P_1^o$	193.4048	-1.85	0.083	0.0589(29)	0.0685(47)	-1.94	
$^3P_2$-$^1P_1^o$	194.4118	-1.44	0.208	0.0161(18)	0.0164(20)	-2.55	
$^3P_1$-$^3P_0^o$	194.4730	-1.15	1.238	1.000	1.25(16)	-1.15	-1.40[c]
$^3P_2$-$^1F_3^o$	195.3805	-2.39	0.010	0.746(150)$\times10^{-3}$	1.96(42)$\times10^{-3}$	-3.11	
$^3P_1$-$^3P_1^o$	195.5115	-1.19	0.375	0.370(10)	0.430(23)	-1.13	-1.33[c]
$^3P_1$-$^3P_2^o$	196.5384	-1.68	0.071	0.0186(9)	0.0248(20)	-2.14	
$^3P_2$-$^3P_1^o$	198.8268	-1.20	0.351	0.354(10)	0.412(22)	-1.14	-1.35[c]
$^3P_2$-$^3P_2^o$	199.8887	-0.44	1.195	0.932(6)	1.24(8)	-0.43	-0.78,[c] -0.24[d]
$^3P_1$-$^3F_2^o$	201.9068	-0.85	0.470	0.674(24)	0.515(27)	-0.80	-0.63[d]
$^3P_0$-$^3D_1^o$	204.1712	-0.55	1.500	0.672(17)	1.56(15)	-0.53	-0.70,[c] -0.44,[d] -0.84[f]
$^3P_2$-$^3F_3^o$	204.3770	-0.49	0.740	0.931(10)	0.862(41)	-0.42	-0.51,[d] -0.61,[f] -0.67[g]
$^3P_2$-$^3F_2^o$	205.4461	-1.33	0.150	0.166(8)	0.127(8)	-1.40	-1.02[d]
$^3P_1$-$^3D_1^o$	206.5215	-0.83	0.764	0.314(16)	0.730(77)	-0.85	-0.77,[c] -0.81,[d] -0.86,[f] -0.91[g]
$^3P_1$-$^3D_2^o$	206.8656	-0.35	1.388	0.908(5)	1.49(10)	-0.32	-0.41,[c] -0.28,[d] -0.41,[f] -0.46[g]
$^3P_1$-$^1D_2^o$	208.6021	-1.16	0.209	0.198(20)	0.150(16)	-1.31	-0.90,[c] -0.99[d]
$^3P_2$-$^3D_3^o$	209.4258	-0.12	1.643	0.975(5)	1.63(11)	-0.12	-0.35,[c] -0.22,[d] -0.16,[f] -0.21[g]
$^3P_2$-$^3D_1^o$	210.2265	-2.52	0.015	0.0040(4)	0.0093(13)	-2.73	-0.89[g]
$^3P_2$-$^3D_2^o$	210.5824	-1.09	0.242	0.0896(45)	0.147(12)	-1.31	-1.24,[c] -1.09[d]
$^3P_2$-$^1D_2^o$	212.3825	-2.72[e]	0.0056[e]	0.0404(40)	0.0306(34)	-1.99	
$^1D_2$-$^1P_1^o$	218.6451	-1.97	0.048	0.172(12)	0.176(15)	-1.42	
$^1D_2$-$^1F_3^o$	219.8714	0.12	2.609	0.9993(1)	2.63(21)	0.13	-0.16,[d] 0.11,[f] 0.07[g]
$^1D_2$-$^3P_1^o$	224.247	-2.11	0.035	0.139(10)	0.162(14)	-1.44	
$^1D_2$-$^3P_2^o$	225.6001	-1.68	0.055	0.0494(50)	0.0659(92)	-1.60	-1.92,[c] -1.20,[d] -1.32,[f] -1.38[g]
$^1D_2$-$^3F_3^o$	231.4201	-1.02	0.171	0.0694(104)	0.0643(100)	-1.44	-0.95,[d] -1.26,[f] -1.32[g]
$^1D_2$-$^3F_2^o$	232.7918	-1.28	0.131	0.160(16)	0.122(13)	-1.30	-0.78,[d] -1.25,[f] -1.28[g]
$^1D_2$-$^3D_3^o$	237.9144	-1.84	0.241	0.0254(50)	0.0423(89)	-1.60	-0.65,[d] -1.30,[f] -1.35[g]

TABLE III. (*Continued*).

| | HFR | | | Experiment | | | |
Transition	λ (expt.)[a] (nm)	$\log_{10}gf$	A (10^8 s^{-1})	BR	A (10^8 s^{-1})	$\log_{10}gf$	Previous $(\log_{10}gf)$
$^1D_2$-$^3D_1^o$	238.9473	-2.21	0.023	0.0057(14)	0.0133(35)	-2.47	
$^1D_2$-$^3D_2^o$	239.4080	-2.67	0.0050	0.0200(30)	0.00328(54)	-2.85	
$^1D_2$-$^1D_2^o$	241.7367	-0.62	0.539	0.761(24)	0.577(36)	-0.60	-0.31,[c] 0.28,[d] -0.40,[h] -0.59,[f] -0.63[g]
$^1S_0$-$^1P_1^o$	274.0426	-0.81	0.444	0.778(10)	0.794(44)	-0.57	0.44[d]
$^1S_0$-$^3P_1^o$	282.9008	-0.96	0.309	0.0778(78)	0.090(10)	-1.49	-0.92,[c] -0.29,[d] -1.30[g]
$^1S_0$-$^3D_1^o$	306.7021	-1.98	0.024	0.0040(10)	0.0093(24)	-2.41	0.49[d]

[a]From Andrew and Meissner [35]. The wavelengths are given in air above 200 nm and in vacuum below that limit.
[b]Wavelengths calculated on the basis of the energy levels of Sugar and Musgrove [6].
[c]Lotrian *et al.* [41] (emission measurements).
[d]Corliss and Bozman [42] (arc measurements).
[e]Cancellation factor, as defined by Cowan [36], $|CF| < 0.0050$.
[f]Pokrzywska *et al.* [44] (wall stabilized arc).
[g]Musiol *et al.* [45] (wall-stabilized arc measurements).
[h]Slavenas [43] [hook method: the relative values have been normalized to $\lambda = 303.9067$ nm ($\log_{10}gf = -0.07$)].

neutral germanium by considering the time-resolved UV laser-induced fluorescence emitted from a laser-produced plasma. Branching ratios have been determined using inductively coupled plasma emission spectrometry. The lifetimes and branching ratios have been combined in order to deduce a set of accurate experimental transition probabilities. The HFR approach, taking configuration-interaction and polarization effects into account, has also been combined with a least-square fitting procedure of the calculated eigenvalues of the Hamiltonian to the observed energy levels in order to provide an independent set of transition probabilities. Good agreement between the experimental and the semiempirical transition probability values, calculated with the optimized parameters and normalized to the laser measurements, has

been achieved except for a few weak intercombination transitions.

[1] Z.-S. Li, S. Svanberg, E. Biémont, P. Palmeri, and Jiang Zhankui, Phys. Rev. A **57**, 3443 (1998).

[2] S. Adelman, W. P. Bidelman, and D. Pyper, Astrophys. J. **40**, 371 (1979).

[3] D. S. Leckrone, S. G. Johansson, and G. N. Wahlgren, *The First Year of HST Observations*, edited by A. L. Kinney and J. C. Blades (Space Telescope Science Institute, Baltimore, 1991).

[4] C. E. Moore, M. G. J. Minnaert, and J. Houtgast, *The Solar Spectrum 2935–8770 Å*, Natl. Bur. Stand. (U.S.) Monograph 61 (U.S. GPO, Washington, DC, 1966).

[5] E. Biémont, C. Lyngå, Z. S. Li, S. Svanberg, H. P. Garnir, and P. S. Doidge, Mon. Not. R. Astron. Soc. **297**, 713 (1998).

[6] J. Sugar and A. Musgrove, J. Phys. Chem. Ref. Data **22** (5), 1216 (1993).

[7] C. M. Brown, S. G. Tilford, and M. L. Ginter, J. Opt. Soc. Am. **67**, 584 (1977).

[8] G. J. Humphreys and K. L. Andrew, J. Opt. Soc. Am. **54**, 1134 (1964).

[9] G. M. Lawrence, Astrophys. J. **148**, 261 (1967).

[10] T. Andersen, A. P. Petkov, and G. Sorensen, Phys. Scr. **12**, 283 (1975).

[11] V. A. Komarovskii and Ya. F. Verolainen, Opt. Spektrosk. **66**, 507 (1989) [Opt. Spectrosc. **66**, 294 (1989)].

[12] K. Tint, A. Kono, and T. Goto, J. Quant. Spectrosc. Radiat. Transf. **43**, 427 (1990).

[13] L. Holmgren and S. Garpman, Phys. Scr. **10**, 215 (1974).

[14] J. Norin, Diploma thesis, Lund Institute of Technology, 1998 (unpublished).

[15] R. R. Chiao, C. H. Townes, and B. P. Stoicheff, Phys. Rev. Lett. **12**, 592 (1964).

[16] D. T. Hon, Opt. Lett. **5**, 516 (1980).

[17] M. J. Damzen and M. H. R. Hutchinson, Opt. Lett. **8**, 313 (1983).

[18] R. Fedosejevs and A. A. Offenberger, IEEE J. Quantum Electron. **QE-21**, 1558 (1985).

[19] C. B. Dane, W. A. Neuman, and L. A. Hackel, IEEE J. Quantum Electron. **30**, 1907 (1994).

[20] C. B. Dane, L. E. Zapata, W. A. Neuman, M. A. Norton, and L. A. Hackel, IEEE J. Quantum Electron. **31**, 148 (1995).

[21] S. Schiemann, W. Ubachs, and W. Hogervorst, IEEE J. Quantum Electron. **33**, 358 (1997).

[22] S. Schiemann, W. Hogervorst, and W. Ubachs, IEEE J. Quantum Electron. **34**, 407 (1998).

[23] J. Bengtsson, J. Larsson, S. Svanberg, and C.-G. Wahlström, Phys. Rev. A **41**, 233 (1990).

[24] G. J. Bengtsson, P. Jönsson, J. Larsson, and S. Svanberg, Z. Phys. D **22**, 437 (1991).

[25] Luo Caiyan, U. Berzinsh, R. Zerne, and S. Svanberg, Phys. Rev. A **52**, 1936 (1995).

[26] U. Berzinsh, Luo Caiyan, R. Zerne, and S. Svanberg, Phys. Rev. A **55**, 1836 (1997).

[27] Z. S. Li, A. Persson, S. Svanberg, H. P. Garnir, and E. Biémont, Eur. Phys. J. D **2**, 11 (1998).

[28] S. Hashiguchi and M. Hasikuni, J. Phys. Soc. Jpn. **54**, 1290 (1985).

[29] W. Whaling, M. T. Carle, and M. L. Pitt, J. Quant. Spectrosc. Radiat. Transf. **50**, 7 (1993).

[30] A. Siems, J. P. Knauer, M. Kock, S. Johansson, and U. Litzén, J. Quant. Spectrosc. Radiat. Transf. **56**, 513 (1996).

[31] D. E. Blackwell, A. J. Booth, A. D. Petford, and J. M. Laming, Mon. Not. R. Astron. Soc. **236**, 235 (1989).

[32] D. E. Blackwell, A. D. Petford, and G. J. Simmons, Mon. Not. R. Astron. Soc. **201**, 595 (1982), and references therein.

[33] T. R. O'Brian, M. E. Wickliffe, J. E. Lawler, W. Whaling, and J. W. Brault, J. Opt. Soc. Am. B **8**, 1185 (1991).

[34] P. S. Doidge (unpublished).

[35] K. L. Andrew and K. W. Meissner, J. Opt. Soc. Am. **49**, 146 (1959).

[36] R. D. Cowan, *The Theory of Atomic Structure and Spectra* (University of California Press, Berkeley, 1981).

[37] J. Migdalek and W. E. Baylis, J. Phys. B **11**, L497 (1978).

[38] P. Quinet, P. Palmeri, and E. Biémont, J. Quant. Spectrosc. Radiat. Transf. (to be published).

[39] E. Biémont, J.-F. Dutrieux, I. Martin, and P. Quinet, J. Phys. B **31**, 3321 (1998).

[40] S. Fraga, J. Karwowski, and K. M. S. Saxena, *Handbook of Atomic Data* (Elsevier, Amsterdam, 1976).

[41] J. Lotrian, J. Cariou, Y. Guern, and A. Johannin-Gilles, J. Phys. B **11**, 2273 (1978).

[42] C. H. Corliss and W. R. Bozman, *Experimental Transition Probabilities for Spectral Lines of Seventy Elements*, Natl. Bur. Stand. (U.S.) Monograph 53 (U.S. GPO, Washington, DC, 1962).

[43] J. J. Slavenas, Opt. Spectrosc. **16**, 214 (1964).

[44] B. Pokrzywska, K. Musiol, M. Stanek, and S. Labuz, Acta Phys. Pol. A **68**, 763 (1985).

[45] K. Musiol, B. Pokrzywska, E. Pawelec, and M. Rusin, in *Proceedings of the Fifth International Colloquium on Atomic Spectra and Oscillator Strengths for Astrophysical and Laboratory Plasmas*, edited by W.-U. L. Tchang-Brillet, J.-F. Wyart, and C. J. Zeippen (Publication de l'Observatoire de Meudon, Meudon, 1996), p. 36.

[46] E. Biémont, M. Baudoux, R. L. Kurucz, W. Ansbacher, and E. H. Pinnington, Astron. Astrophys. **249**, 539 (1991).

[47] E. H. Pinnington, Q. Li, B. Guo, R. W. Berends, J. Van Hunen, and E. Biémont, Can. J. Phys. **71**, 470 (1993).

[48] E. Biémont, E. H. Pinnington, J. A. Kernahan, and G. Rieger, J. Phys. B **30**, 2067 (1997).